

Mimusops elengi Phytoconstituents *In-silico* Prediction for Alzheimer Disease

Research Article

**Shilpa S Borkar^{1*}, Ashwini Manjrekar¹, Satish S Meshram², Ketki A Bhatt¹,
Amar H Deshpande¹, Jagdish R Baheti¹, Mohammad Tauqeer Sheikh³**

1. Kamla Nehru College of Pharmacy, Butibori-44110. India.

2. Department of Pharmaceutical Sciences, RTMNU, Nagpur-440033. India.

3. K. C. Bajaj College of Pharmacy & Research, Jaripatka, Nagpur (MS), India.

Abstract

Objective: Alzheimer's disease (AD), which predominantly affects older adults, is the primary cause of dementia, impacting 46 million people worldwide. By 2030 and 2050, respectively, there will be 74.7 and 131.5 million persons with AD, as the incidence rises exponentially every five years. The goals of treatment are to control symptoms, lessen clinical decline, and manage the burden of illness. Our study included in-silico testing of the phytoconstituents of *Mimusops elengi* for immunosuppressive effectiveness in the treatment of Alzheimer's. **Methods:** Molecular docking is performed using Discovery Studio to evaluate the pattern of interaction between the crystal structure of the malarial proteins (PDB ID: 7UJQ & 7Q8V) and phytoconstituents from the *Mimusops elengi* plant. Swiss ADME and pkCSM were later used to test for both the pharmacokinetic profile and toxicity respectively. **Result:** According to the docking results, quercetin (-8.4 kcal/mol), myricetin (-8.5 kcal/mol), aesculin (-8.1 kcal/mol), and myricitrin (-9.3 kcal/mol) -9.7 kcal/mol for spinasterol Aesculin (-7.7 kcal/mol), Quercetin (-9.3 kcal/mol), Myricitrin (-9.9 kcal/mol), and Catechin (-8.2 kcal/mol) for 7UJQ macromolecule -8.2 kcal/mol of spinasterol The 7Q8V macromolecule's catechin (-9.1 kcal/mol) had the best binding to immunosuppressive action when compared to all other standards. Additionally, ADMET experiments showed that the pharmacokinetics and toxicity parameters were within acceptable bounds. **Conclusions:** The binding potential of phytoconstituents with an eye toward immunosuppressive function showed promising results. Along with providing important information on clinical treatment and pharmaceutical research, it encourages the use of *Mimusops elengi*.

Keywords: *Mimusops elengi*, In-silico study, Alzheimer disease, Docking, Immunosuppressant.

Introduction

Alzheimer's disease (AD), the leading neurological cause of dementia, affects more than 46 million people worldwide primarily older adults. According to estimates by 2030, 74.7 million people will have AD, and by 2050, 131.5 million as the disease's incidence rises exponentially every five years beyond the age of 65 (1).

Progressive memory loss, diminished cognitive function, and ultimately dementia is experienced by patients with AD. The neuropathological hallmarks of AD include intracellular neurofibrillary tangles of hyperphosphorylated tau protein, loss of synaptic connections, neuronal degeneration, with the development of senile plaques outside of cells as a result of amyloid- β (A β) aggregation, which is typically linked to local inflammation and neurite dystrophy/swelling (2). As of right now, AD has no known cure or treatment (3).

Cognitive and behavioral decline in individuals over 65 is a hallmark of dementia. The most prevalent neurological condition, Alzheimer's disease (AD), affects about 24 million individuals globally, and by 2050, that number is expected to have tripled (4).

Acetylcholine (ACh) deficiency and elevated glutamatergic transmission resulting in oxidative damage are also linked to AD (2)(3)(4)(5)(6).

The pathogenesis of Alzheimer's

Progressive brain dysfunction that appears to be staged in a cell biology sequence—neuronal injury, synaptic failure, and neuronal death is a hallmark of AD and associated dementias. AD's pathological hallmarks are neuropil threads and neurofibrillary tangles (NFT). Under a microscope, amyloid plaques, also known as senile plaques, are amorphous aggregates of A β . Additionally, hyperphosphorylated Tau protein accumulates, suggesting the production of neurofibrillary tangles and widespread neuronal death. The pathophysiology of Alzheimer's disease can result from mitochondrial failure because they are engaged in many bodily cellular functions, including signal transmission and neural synapses. Neurodegeneration may result from the development of free radicals and an oxidative stress state within the cells. Given these functions of mitochondria in the pathophysiology of

* Corresponding Author:

Shilpa S Borkar

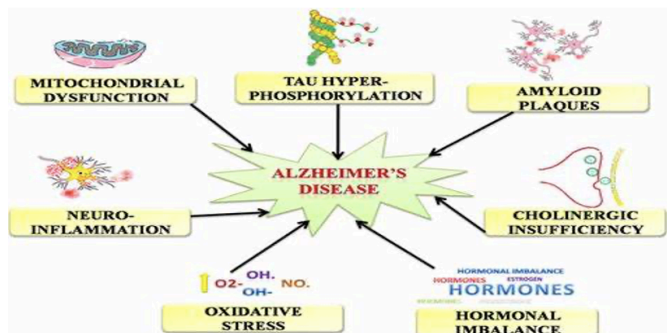
Kamla Nehru College of Pharmacy,
Butibori-44110.

India.

Email Id: preetshilpa81@gmail.com

Alzheimer's disease, the mitochondrial cascade theory was developed, which unambiguously links abnormalities in mitochondria to the etiology of Alzheimer's disease(7).

Figure 1: Pathophysiology of Alzheimer Diseases



Treatment of Alzheimer's Disease

There is no recognized cure for AD dementia. The complex and poorly understood pathological processes that cause AD dementia are increasingly recognized to begin decades before clinical symptoms manifest. By then, extensive and likely irreversible processes have likely caused extensive damage on a number of levels, including molecular, intracellular, network, and system. The current paradigm for treating AD includes many symptom management strategies to maintain quality of life, reduce the burden of illness, and avoid long-term clinical decline. efficient long-term treatment using FDA-approved AD medications. The establishment, application, and upkeep of a solid foundation of psychoeducation, behavioral and nonpharmacological care techniques, and clarity in care objectives and expectations all depend on a strong therapeutic relationship between the therapist and the patient-caregiver dyad. This involves cholinesterase inhibitor (ChEI) monotherapy at first, followed by additional dual-combination treatment with a ChEI and memantine (8).

Mimusops Elengi

The Sapotaceae family includes *Mimusops elengi*, often known as Spanish Cherry, Bullet Wood, Bunga Mengkula, or Mengkulah. Widely distributed throughout South Asian nations, this tropical evergreen shrub is significant in traditional medicine, particularly in Ayurveda, where different plant components are used for their therapeutic qualities. Due to its diverse pharmacological benefits, *Mimusops elengi* is a valuable resource in traditional healing practices (9). The World Health Organization (WHO) claims that approximately two-thirds of the global population relies on traditional medicine for treating various ailments, with *Mimusops elengi*, also known as the Indian Medlar Tree or Bakul tree, being a significant example (10). *Mimusops elengi* is regarded as a sacred plant by Hindus and holds significant importance in religious texts and ancient Sanskrit literature. Its aromatic flowers are praised in the Puranas and are even included among the flowers of Hindu paradise(11).

In Banda Aceh, Indonesia, *Mimusops elengi* serves as a source of agricultural residue biomass. This species has been in the archipelago for ages and is indigenous to India, Myanmar, and Sri Lanka(12)(13) (14). Currently, Banda Aceh has approximately 6,500 *Mimusops elengi* trees spread over 28.2 hectares(15). According to published research, the roots, bark, leaves, flowers, and foliage of the *Mimusops elengi* plant have all been thoroughly examined for potential therapeutic use with encouraging outcomes. It could also be applied to the manufacturing of biodiesel(16)(17).

Historically, *M. elengi* has been used as a tonic and astringent, particularly for the treatment of dysentery and diarrhea due to its ability to tighten and tone tissues. Recent studies have also identified antioxidant properties in its leaves, which are essential for combating harmful free radicals associated with various illnesses and the aging process. Additionally, investigation indicates that *M.elengi* might be beneficial because of its anti-diabetic properties. Diabetics regulate their blood sugar levels. Numerous pharmacological characteristics of *Mimusops elengi* point to both its usefulness in traditional medicine and its potential for use in contemporary medicine in the future. It is crucial to remember that additional research is necessary to completely examine its properties and possible uses in medicine. Before utilizing herbal treatments for health reasons, particularly if you already have health problems or are on additional prescription drugs, always get medical counsel(18).

Plant description

The medium- to large-sized *Mimusops elengi* tree can grow to a height of 25–30 m (82–98 ft). Its crown is straight and its trunk is upright. The evergreen leaves are simple and alternate. They can have an elliptical or oblong shape and are normally 2.4–4.7 inches (6–12 cm) in length. The leaves are glossy and dark green. One of the most notable characteristics of *Mimusops elengi* is its extremely scented blossoms. They resemble stars, have a cream to light yellow tone, and have a waxy touch. The flowers have a sweet and pleasant perfume and are often seen alone or in tiny groups. Blossoming typically occurs in the summer. *Mimusops elengi* produces a green, meaty berry as its fruit. *Mimusops elengi* produces meaty berries that are green while young and turn yellow or orange when ripe. Depending on the age of the tree, its grayish-brown bark may be smooth or rough. Its wood is used for many purposes, like as carving and furniture construction, and is prized for its tensile strength. Because of its extensive root system, the tree may thrive in a wide range of soil types. The *Mimusops elengi* is found in South and Southeast Asia is found in countries such as Thailand, Myanmar, Sri Lanka, India, and so forth. Throughout the world, in many tropical and subtropical areas, it is also grown as an ornamental tree. In addition to its usual medical uses, The wood of *Mimusops elengi* is prized, and aromatic blooms (19) (20)(21)(22). The different phytoconstituents in *M.elengi* are Myricitrin, Myricetin, Quercetin,

Coumarin, and phenolic acids like Aesculin, and Quinic acid. Steroid (Spinasterol), Tannis and Catechin.

Materials and technique

Platform for molecular docking

With Tau protein as the target and the N-methyl D-aspartate (NMDA) receptor as the ligand, a computational docking study of all the phytoconstituents selected as ligands was carried out using PyRx software (26).

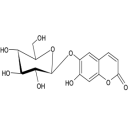
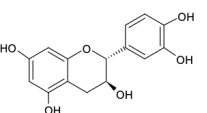
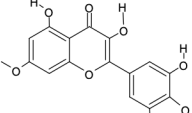
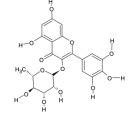
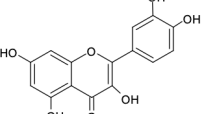
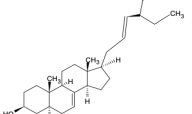
Preparing proteins

The macromolecule is 7UJQ and 7Q8V were examined using *in silico* methods for particular phytoconstituents. determination: 2.05 Å, R-Value Free: 0.244, R-Value Work: 0.194, R-Value Observed: 0.196), The protein data bank (<https://www.rcsb.org>) provided the information. 4RAC belongs to the group of drugs known as transferase/transferase inhibitors. All other molecules were removed, along with undesirable chains, co-crystallized water molecules, and nonstandard residues, utilizing Discovery Studio v.24 and PDB 7UJQ and 7Q8V macromolecule validation.

Ligand preparation

Avogadro software was used to extract the three-dimensional (3D) structures of all constituents from the NCBI website's PubChem database (<https://pubchem.ncbi.nlm.nih.gov/>). Nonetheless, the geometrical 2D structure was drawn using the ChemSketch program. The Avogadro program was used to transform the two-dimensional (2D) ligand structures into three-dimensional (3D) models once they were saved in the PDB format. All of the chemical structures are shown in Figure 2.

Table 1: Chemical structures for each of the chosen phytoconstituents

Aesculin	Catechin	Myricetin
		
Myricitrin	Quercetin	Spinasterol
		

Standard Preparation

The standard is prepared steps like the two-dimensional structure of standard drug was made using chem sketch program, then the two-dimensional structure was converted Avogadro software was used to convert it into a 3D model, and the PDB file was saved. By utilizing PyRx molecular docking of N-methyl D-aspartate (NMDA) receptor and Tau protein was done with 7UJQ and 7Q8V.

Docking of molecules

In order to forecast the ligand molecule's binding affinity, Protein-ligand interactions are evaluated by molecular docking, which also computes the scoring function according to the geometry (27, 28). The way certain phytoconstituents bind (Figure 1) and the standard medication, as well as the crystal structure of the immunosuppressive activity macromolecule (PDB ID: 7UJQ and 7Q8V), were examined using molecular docking experiments. Binding affinity was examined using the Vina wizard tool, while PyRx software was used to conduct the study of molecular docking as a standard, The 2020 Discovery Studio Client was utilized to analyse and illustrate the final data with bound ligands. Protein-ligand interaction visualization shows how many interactions and active residues are responsible for a considerable amount of binding at the active site of the target enzyme.

Predicting Absorption, distribution, metabolism, excretion, and toxicity (ADMET)

Applying the rule of Lipinski, the chosen Citations and phytoconstituents medication were investigated further for drug-likeness characteristics. Before being ingested by humans and animals, the acceptability of Phytochemicals needs to be predicted during the medication development process. The ligands' pharmacokinetic profile (ADME) and toxicity were predicted using SwissADME (<http://www.swissadme.ch>) and pkCSM (<http://biosig.unimelb.edu.au/pkcsmprediction>), an online server database that uses graph-based signatures to predict small-molecule pharmacokinetic features. To examine the toxicological characteristics of ligands, PDB files or simplified molecular input line entry system (SMILES) notations were uploaded. After that, the appropriate models were selected to produce a multitude of data about effects associated with structures (29, 30).

Outcomes and Conversations

The current investigation sought to determine whether the phytoconstituents found in *Mimusops elengi* could reduce immunosuppressive function. In order to investigate the active ingredients inhibitory potentials, we first used Auto Dock Vina to undertake research using molecular docking of every phytoconstituent found in *Mimusops elengi*. Next, we looked at interacting amino acid residues. The servers pkCSM and SwissADME were utilized. To further assess the selected phytoconstituents' absorption, distribution, metabolism, excretion, and toxicity (ADMET) properties showed the best fit.

Docking of molecules

Table 2 shows each chemical component's docking scores and binding energies. *Mimusops elengi* targets immunosuppressive activity (PDB ID: 7UJQ and 7Q8V) as well as binding relationships with residues of amino acids.

Table 2: Immunosuppressive activity-targeting ligand binding interaction from *Mimusops elengi* (PDB ID: 7UJQ and 7Q8V)

Sr.No.	Chemical constituent	Pub Chem ID	Docking score (binding affinity kcal/mol)	
			7UJQ	7Q8V
1	Myricitrin	330.00	-9.3	-9.9
2	Myricetin	205.16	-8.5	-8.8
3	Aesculin	328.23	-8.1	-7.7
4	Quercetin	179.64	-8.4	-9.3
5	Spinasterol	372.21	-9.7	-8.2
6	Catechin	261.03	-8.2	-9.1

7UJQ

The range of phytoconstituents' binding affinities was -9.7 to -8.1 kcal/mol. Compared to other docked compounds, such as Aesculin (-8.1 kcal/mol), Myricitrin (-9.3 kcal/mol), Myricetin (-8.2 kcal/mol), Quercetin (-8.4 kcal/mol), and Catechin (-8.2 kcal/mol), it is clear from the docked results that spinasterol has the most favorable binding affinity (-9.7 kcal/mol) and in complex with selected macromolecules (PDB ID: 7UJQ). demonstrated the substantial role of a variety of interactions, including hydrophobic interactions, π - π stacking, π -alkyl and alkyl interactions, and hydrogen bonding, in the stability of the phytoconstituents' binding to 7UJQ. Additionally, the number of closest amino acid residues, the binding energy of ligand 7UJQ stable complexes, and the number of intermolecular hydrogen bonds were ascertained. selected compound Myricitrin, Myricetin, Quercetin, Aesculin, Spinasterol, Catechin (Table 3).

An investigation of the interaction between the 7UJQ complex of proteins. Myricitrin, Myricetin, Quercetin, Aesculin, Spinasterol, Catechin ligand was also carried out, which demonstrated that the ligand molecule is orientated due to van der Waals interaction with amino acid residue GLU A:96, GLU A:139, GLY A:20, UZD A:301, LYS A:137, GLU B:139, LYS B:21, GLY B:20, ARG C:1300, GLN D:1301, HIS D:1302, ASN A: 135, GLU A: 139, GLY A:20, GLU A: 18, GLY B: 20, SER C: 1303, GLN C: 1301, ARG C: 1300, HIS D:1302, LYS A: 137, GLU A: 139, GLY A:20, UZD B: 301, GLY B: 20, HIS C: 1302, ARG D: 1300, HIS D: 1302, GLU A: 216, LEU A: 221, GLN A: 218, THR A:176, PRO A: 177, LEU B: 159, PHE B:24, LYS C:1297, ARG C: 1299, GLN C: 1301, HIS C: 1302, HIS D: 1302, TYR D: 1304, GLY A: 20, LYS A: 137, GLY B: 20, UZD B: 301, GLN C:1301, HIS C: 1302, HIS D: 1302, ARG D: 1300, GLU A: 139, LYS A: 137, ASN A: 135, ASP A: 156, UZD A: 301, GLY A: 20, GLY B:20, GLU B: 139, LYS B: 137, GLU B: 96, ASN B: 140, HIS C: 1302, ARG C:1300, GLN D:1301, ARG D: 1300, HIS D: 1302 were found (Fig.3).

Analysis of the interactions between the ligand Aesculin and the 7UJQ protein complex revealed that the ligand molecule is orientated as a result of pi-alkyl interactions with amino acid residues ARG D:1300 and the formation of traditional hydrogen bonds with LYS A:21, GLN C:1301, HIS C:1302, LYS B:137 residues and In addition, Eleven interactions between amino acid

residues and van der Waals GLU A:96, GLU A:139, GLY A:20, UZD A:301, LYS A:137, GLU B:139, LYS B:21, GLY B:20, ARG C:1300, GLN D:1301, HIS D:1302, were found (Fig. 3).

Analysis of interactions between the ligand Catechin and the 7UJQ protein complex revealed that ligand molecule is orientated as a result Pi-alkyl interactions with amino acid residues LYS B:21, LYS A:21 and Pi-cation interaction with LYS A:137 and forming conventional hydrogen bonds with ASN A: 140, ASP A: 156, HIS C: 1302 residues and In addition, Nine interaction between amino acid residues and van der Waals ASN A: 135, GLU A: 139, GLY A:20, GLU A: 18, GLY B: 20, SER C: 1303, GLN C: 1301, ARG C: 1300, HIS D:1302 were found (Fig. 3).

Analysis of interactions between the ligand Myricitin and the 7UJQ protein complex revealed that ligand molecule is orientated as result Pi-alkyl interactions with amino acid residues ARG C:1300 and Pi-anion interaction with GLU A:96, Pi-sigma interaction LYS A:21 and forming conventional hydrogen bonds with LYS A: 21, UZD A: 301, LYS B:21, GLN C: 1301 residues and In addition, Eight interaction between amino acid residues and van der Waals LYS A: 137, GLU A: 139, GLY A:20, UZD B: 301, GLY B: 20, HIS C: 1302, ARG D: 1300, HIS D: 1302 were found (Fig. 4).

Analysis of interactions between the ligand Myricitrin and the 7UJQ protein complex revealed that the ligand molecule is oriented as a result of Pi-alkyl interactions with amino acid residues ARG C:1300, Pi-anion interaction with GLU A:96, and Pi-sigma interaction with LYS A:21. It also forms conventional hydrogen bonds with LYS A:21, UZD A:301, LYS B:21, and GLN C:1301 residues. In addition, eight van der Waals interactions were observed with amino acid residues LYS A:137, GLU A:139, GLY A:20, UZD B:301, GLY B:20, HIS C:1302, ARG D:1300, and HIS D:1302. Notably, non-amino acid interactions involving UZD moieties (UZD A:301 and UZD B:301) further stabilized the ligand binding, indicating the contribution of prosthetic group components or cofactors present in the protein complex. These interactions collectively contribute to the stabilization and specificity of ligand binding within the active site of the 7UJQ complex (Fig. 5).

Analysis of the interactions between the ligand Myricitrin and the 7UJQ protein complex revealed that the molecules is orientated as result of Pi-alkyl interaction with amino acid residues ALA B:23, Pi-anion interaction with LYS B:56, Pi-cation interaction with ASP D:1305 conventional hydrogen bonds interactions with the amino acid residues ASP A:215, TYR C:1304, SER D: 1303, ASP D: 1305. In addition, Thirteen van der Waals interactions with amino acid residues GLU A: 216, LEU A: 221, GLN A: 218, THR A:176, PRO A: 177, LEU B: 159, PHE B:24, LYS C:1297, ARG C: 1299, GLN C: 1301, HIS C: 1302, HIS D: 1302, TYR D: 1304 were found (Fig. 6).

Analysis of the interactions between the ligand Quercetin and the 7UJQ protein complex revealed that the molecules is orientated as result of Pi-alkyl

interaction with amino acid residues ARG C:1300, Pi-anion interaction with GLU A:96, Pi-sigma interaction with LYS A:21 conventional hydrogen bonds interactions with the amino acid residues GLU A: 139, UZD A: 301, LYS A: 21. In addition, Thirteen van der Waals interactions with amino acid residues GLY A: 20, LYS A: 137, GLY B: 20, UZD B: 301, GLN C:1301, HIS C: 1302, HIS D: 1302, ARG D: 1300 were found (Fig. 7).

An analysis of the interactions between the ligand Spinasterol and the 7UJQ protein complex revealed that the molecules is orientated as result of Pi-alkyl interaction with amino acid residue LYS A:21, LYS B:21 Unfavorable Donar Donar interaction with ASN A:140 Unfavorable acceptor-acceptor with SER C:1303. In addition, Sixteen van der Waals interactions with amino acid residues GLU A: 139, LYS A: 137, ASN A: 135, ASP A: 156, UZD A: 301, GLY A: 20, GLY B:20, GLU B: 139, LYS B: 137, GLU B: 96, ASN B: 140, HIS C: 1302, ARG C:1300, GLN D:1301, ARG D: 1300, HIS D: 1302 were found (Fig. 8).

7Q8V

The phytoconstituents' binding affinities varied from -9.9 to -7.7 kcal/mol. In comparison to other docked compounds, such as Aesulin (-7.7 kcal/mol), Spinasterol (-8.2 kcal/mol), Myricetin (-8.8 kcal/mol), Quercetin (-9.3 kcal/mol), and Catechin (-9.1 kcal/mol), it is clear from the docked results that Myricitrin exhibits the most favorable binding affinity (-9.9 kcal/mol) and in complex with selected macromolecules (PDB ID: 7Q8V). A visual inspection of the computationally docked optimal binding poses of phytoconstituents on selected macromolecules (i.e. 7Q8V). demonstrated that the stability of the phytoconstituents' binding to 7Q8V was significantly influenced by a variety of interactions, including hydrogen bonding and hydrophobic interactions, such as π - π stacking and π -alkyl and alkyl interactions.

Additionally, the number of closest amino acid residues, the binding energy of ligand 7Q8V stable complexes, and the number of intermolecular hydrogen bonds were ascertained. selected compound Myricitrin, Myricetin, Quercetin, Aesculin, Spinasterol, Catechin (Table 2).

An investigation of the interaction between the 7Q8V complex of proteins. Myricitrin, Myricetin, Quercetin, Aesculin, Spinasterol, Catechin ligand was also carried out, which demonstrated that the ligand molecule is orientated due to van der Walls interaction with amino acid residue LEU A: 179, GLY A: 178, VAL A: 73, PHE A: 45, GLU A: 77, LEU A: 74, GLY A: 46, GLU A: 65, LYS A:63, ASP A: 176, ILE A: 48, ASN A: 159 ASP A: 176, ILE A: 48, GLU A: 47, LEU A: 74, GLY A: 46, GLU A: 65, GLN A: 69, VAL A: 73, GLY A: 178, LYS A: 156, SER A: 158, ASN A: 159 GLY A:42, ILE A:48, VAL A:64, LEU A:74, GLU A:65, GLN A:69, VAL A:73, LEU A:179, GLY A:178, ASN A:159, LEU A:175, SER A:158, LYS A:156, LEU A:175, ASN A:113, LYS A:156, THR A:202, LEU A:179, GLY A:201, GLY A:44, GLY A:178, VAL A:73, GLU A:65, GLY A:46, LEU A:74, ILE A:48, ASN

A:159, ASN A:113, LYS A:156, GLY A:178, LEU A:74, VAL A:73, GLY A:46, GLU A:65, GLU A:77, LEU A:74, VAL A:73, GLU A:65, GLY A:46, GLY A:43, PHE A:45, GLY A:42, ASN A:159, SER A:158, ARG A:119, ALA A:115, THR A:202, LYS A:156, ASP A:176, GLY A:178 were found (Fig No. 9)

Analysis of the interactions between the ligand Aesculin and the 7Q8V protein complex revealed that the ligand molecules are oriented due to one Pi-alkyl interaction with amino acid residues A:9IV402, Pi-cation interaction with LYS A:156, Pi-sigma interaction with A:9IV402 conventional hydrogen bonds interactions with the amino acid residues LYS A: 156, SER A: 158, VAL A: 64, GLU A: 47 U Carbon Hydrogen Bond interaction with GLU A:77, ASP A:176. In addition, ten interactions between amino acid and van der Waals LEU A: 179, GLY A: 178, VAL A: 73, PHE A: 45, LEU A: 74, GLY A: 46, GLU A: 65, LYS A:63, ILE A: 48, ASN A: 159 were found (Fig. 9).

An analysis of the interactions between the ligand Catechin and the 7Q8V protein complex revealed that the ligand molecule is oriented due to one Pi-alkyl interaction with amino acid residues A:9IV402, LYS A:63 Pi-anion interaction with GLU A:77 conventional hydrogen bonds interactions with the amino acid PHE A: 45, VAL A: 64 residues. In addition, twelve interactions between amino acids and van der Waals ASP A: 176, ILE A: 48, GLU A: 47, LEU A: 74, GLY A: 46, GLU A: 65, GLN A: 69, VAL A: 73, GLY A: 178, LYS A: 156, SER A: 158, ASN A: 159 were found (Fig. 10).

An analysis of the interactions between the ligand Myricitin and the 7Q8V protein complex revealed that the ligand molecule is oriented due to one Pi-alkyl interaction with amino acid residues A:9IV402, LYS A:63 Pi-anion interaction with GLU A:77 conventional hydrogen bonds interactions with the amino acid GLU A: 47, PHE A: 45, ASP A: 176 residues Carbon Hydrogen Bond interaction with GLY A:178, ILE A:48, GLY A:42. In addition, Twelve interaction between amino acid and van der Waals VAL A:64, LEU A:74, GLU A:65, GLN A:69, VAL A:73, LEU A:179, ASN A:159, LEU A:175, SER A:158, LYS A:156 were found (Fig. 11).

An analysis of the interactions between the ligand Myricitrin and the 7UJQ protein complex revealed that the ligand molecule is oriented due to one Pi-alkyl interaction with amino acid residues LYS A:63 A:9IV402, Pi-anion interaction with GLU A:77, ASP A:176, Pi-sigma interaction with PHE A:45 conventional hydrogen bonds interactions with the amino acid residues SER A:158, ASN A:159, VAL A:64, GLU A:47, ASP A:154 Unfavourable Acceptor-Acceptor interaction with ASP A:154. In addition, twelve interactions between amino acid and van der Waals LEU A:175, ASN A:113, LYS A:156, THR A:202, LEU A:179, GLY A:201, GLY A:44, GLY A:178, VAL A:73, GLU A:65, GLY A:46, LEU A:74 were found (Fig. 12).

An analysis of the interactions between the ligand Quercetin and the 7UJQ protein complex revealed that the ligand molecule is oriented due to one Pi-alkyl

Shilpa S. Borkar et.al., *Mimusops elengi* Phytoconstituents in-silico Prediction for Alzheimer Disease

interaction with amino acid residues LYS A:63 A:9IV402, Pi-anion interaction with GLU A:77, ASP A:176, conventional hydrogen bonds interactions with the amino acid residues VAL A:64, PHE A:45, SER A:158, Carbon Hydrogen Bond with interaction GLY A:178, Unfavourable Doner-Doner interaction with GLU A:47. In addition, Twelve interactions between amino acid and van der Waals ILE A:48, ASN A:159, ASN A:113, LYS A:156, LEU A:74, VAL A:73, GLY A:46, GLU A:65 were found (Fig. 13).

An analysis of the interactions between the ligand Spinasterol and the 7UJQ protein complex revealed that the ligand molecule is oriented due to one Pi-alkyl interaction with amino acid residues LYS A:63 A:9IV402 Alkyl interaction with ILE A:48. In addition, Sixteen interactions between amino acid and van der Waals GLU A:77, LEU A:74, VAL A:73, GLU A:65, GLY A:46, GLY A:43, PHE A:45, GLY A:42, ASN A:159, SER A:158, ARG A:119, ALA A:115, THR A:202, LYS A:156, ASP A:176, GLY A:178 were found (Fig.14).

Table 3: Binding interaction of ligand with the binding site 7UJQ and 7Q8V

S. No.	Inhibitors	Binding energy(kcal/mol)	H bond	Main amino acid interaction	
				Pi-sulfur, pi-alkyl, pi-sigma, Unfavorable acceptor-acceptor, Unfavorable doner-doner, Pi-cation, Pi-anion	Van der Waals
1	Aesculin	-8.1	LYS B: 137, LYS A: 21, HIS C: 1302, GLN C: 1301	ARG D: 1300	GLU A:96 (0.7A°), GLU A:139, GLY A:20, UZD A:301, LYS A:137, GLU B:139, LYS B:21, GLY B:20, ARG C:1300, GLN D:1301, HIS D:1302 (0.9A°)
2	Catechin	-8.2	ASN A: 140, ASP A: 156, HIS C: 1302	LYS A: 137, LYS A: 21, LYS B: 21	ASN A: 135 (0.7A°), GLU A: 139, GLY A:20, GLU A: 18, GLY B: 20, SER C: 1303, GLN C: 1301, ARG C: 1300, HIS D:1302 (0.6A°)
3	Myricetin	-8.5	LYS A: 21, UZD A: 301, LYS B:21, GLN C: 1301	GLU A: 96, ARG C: 1300	LYS A: 137 (0.7A°), GLU A: 139, GLY A:20, UZD B: 301, GLY B: 20, HIS C: 1302, ARG D: 1300, HIS D: 1302 (1.1A°)
4	Myricitrin	-9.3	ASP A:215, TYR C:1304, SER D: 1303, ASP D: 1305	TRP A: 214, ALA B: 23, LYS B: 56	GLU A: 216 (0.9A°), LEU A: 221, GLN A: 218, THR A:176, PRO A: 177, LEU B: 159, PHE B:24, LYS C:1297, ARG C: 1299, GLN C: 1301, HIS C: 1302, HIS D: 1302, TYR D: 1304 (1.3A°)
5	Quercetin	-8.4	GLU A: 139, UZD A: 301, LYS A: 21	GLU A: 96, LYS B: 21, ARG C: 1300	GLY A: 20, LYS A: 137, GLY B: 20, UZD B: 301, GLN C:1301, HIS C: 1302, HIS D: 1302, ARG D: 1300
6	Spinasterol	-9.7		ASN A: 140, LYS A: 21, LYS B: 21, SER C: 1303	GLU A: 139 (0.8A°), LYS A: 137, ASN A: 135, ASP A: 156, UZD A: 301, GLY A: 20, GLY B:20, GLU B: 139, LYS B: 137, GLU B: 96, ASN B: 140, HIS C: 1302, ARG C:1300, GLN D:1301, ARG D: 1300, HIS D: 1302 (0.2A°)
S. No.	Inhibitor	Binding energy(kcal/mol)	H bond	Main amino acid interaction	
				Pi-sulfur, pi-alkyl, pi-sigma, Unfavorable acceptor-acceptor, Unfavorable doner-doner, Pi-cation, Pi-anion Carbon Hydrogen Bond	Van der Waals
1	Aesculin	-7.7	LYS A: 156, SER A: 158, VAL A: 64, GLU A: 47	A:9IV402, LYS A:156, ASP A:176, GLU A:77	LEU A: 179, GLY A: 178, VAL A: 73, PHE A: 45, LEU A: 74, GLY A: 46, GLU A: 65, LYS A:63, ILE A: 48, ASN A: 159
2	Catechin	-9.1	PHE A: 45, VAL A: 64	GLU A: 77, LYS A: 63, A:9IV402	ASP A: 176, ILE A: 48, GLU A: 47, LEU A: 74, GLY A: 46, GLU A: 65, GLN A: 69, VAL A: 73, GLY A: 178, LYS A: 156, SER A: 158, ASN A: 159
3	Myricetin	-8.8	GLU A: 47, PHE A: 45, ASP A: 176	GLU A: 77, LYS A: 63, A:9IV402, GLY A:178, ILE A:48, GLY A:42	VAL A:64, LEU A:74, GLU A:65, GLN A:69, VAL A:73, LEU A:179, ASN A:159, LEU A:175, SER A:158, LYS A:156

4	Myricitrin	-9.9	SER A:158, ASN A:159, VAL A:64, GLU A:47, ASP A:154	GLU A:77, ASP A:176, LYS A:63, A:91V402, PHE A:45, ASP A:154	LEU A:175, ASN A:113, LYS A:156, THR A:202, LEU A:179, GLY A:201, GLY A:44, GLY A:178, VAL A:73, GLU A:65, GLY A:46, LEU A:74,
5	Quercetin	-9.3	VAL A:64, PHE A:45, SER A:158,	GLU A:77, ASP A:176, GLU A:47, LYS A:63, A:91V402, GLY A:178	ILE A:48, ASN A:159, ASN A:113, LYS A:156, LEU A:74, VAL A:73, GLY A:46, GLU A:65
6	Spinasterol	-8.2		ILE A:48, LYS A:63, A:91V402	GLU A:77, LEU A:74, VAL A:73, GLU A:65, GLY A:46, GLY A:43, PHE A:45, GLY A:42, ASN A:159, SER A:158, ARG A:119, ALA A:115, THR A:202, LYS A:156, ASP A:176, GLY A:178

ADMET Research

When turning a chemical into a powerful medication, the ligands' pharmacokinetic profile (ADME) and toxicity projections are crucial considerations. pkCSM and SwissADME were utilized to assess these parameters in the current investigation. The topological polar surface area (TPSA) and the partition coefficient (Log P) are used to characterize the absorption potential and lipophilicity, respectively. A medication molecule's TPSA should be less than 140 Å for optimal cell membrane penetration. However, the drug target affects the value of Log P. For a number of medications, the optimal Log P value is 1.35 to 1.80 for oral and intestinal absorption, > 5 for sublingual absorption, and 31 for central nervous system (CNS) absorption (23). It is optimal for ligands to have an aqueous solubility between -6.5 and 0.5 (32). whereas the value ranges from -3.0 to 1.2 for the blood-brain barrier (BBB) (33). Drug resistance is also caused by P-glycoprotein which is not a substrate (34). There is no violation of the Lipinski rule as shown in Table 2.

Table 4 legend: *In-silico* kinetic prediction of phytoconstituent from *Mimosups elengii*

ADMET Properties	Formula	MW (g/mol)	Log P	TPSA (Å ²)	HB donor	Hb acceptor	Aqueous Solubility Log mol/L)	Human intestinal absorption (%)	Blood-brain barrier
Aesculin	C ₁₅ H ₁₆ O ₉	340.28	-1.3227	149.82	5	9	-2.871	40.366	-1.186
Catechin	C ₁₅ H ₁₄ O ₆	290.27	1.5461	110.38	5	6	-2.97	66.032	-1.219
Myricetin	C ₁₅ H ₁₀ O ₈	318.24	1.6936	151.59	6	8	-2.979	67.622	-1.803
Myricitrin	C ₂₁ H ₂₀ O ₁₂	464.38	0.1943	210.51	8	12	-2.949	56.935	-2.17
Quercetin	C ₁₅ H ₁₀ O ₇	302.24	1.988	131.36	5	7	-3.18	74.634	-1.481
Spinasterol	C ₂₈ H ₄₆ O	398.66	7.5548	20.23	1	1	-6.56	97.539	0.814

Table 4 legend: *In-silico* kinetic prediction of phytoconstituent from *Mimosups elengii* (continued...)

ADMET Properties	P- glycoprotein substrate	Total clearance [Log mL(min.kg)]	Bioavailability score	AMES toxicity	Max tolerated dose [Log mg/(kg.d)]	hERG 1 inhibitor	hERG 2 inhibitor
Aesculin	Yes	0.751	0.55	No	0.424	No	No
Catechin	Yes	0.224	0.55	No	0.242	No	No
Myricetin	Yes	0.5	0.55	No	0.863	No	No
Myricitrin	Yes	0.501	0.17	Yes	0.662	No	Yes
Quercetin	Yes	0.547	0.55	Yes	0.951	No	No
Spinasterol	Yes	0.659	0.55	No	-0.915	No	No

Table 4 legend: *In-silico* kinetic prediction of phytoconstituent from *Mimosups elengii* (continued...)

ADMET Properties	Acute Oral rat toxicity, LD50 (mol/kg)	Oral rat chronic toxicity (Log mh/kg bw/day)	Hepatotoxicity	Skin sensitization	<i>T. Pyriformis</i> toxicity (Log µg/L)	Minnow toxicity (Log mmol/L)	Lipinski's rule violations
Aesculin	2.714	4.148	Yes	No	0.285	2.959	Yes (0)
Catechin	2.107	1.953	No	No	0.405	1.7	Yes (0)
Myricetin	2.854	2.811	No	No	0.288	0.942	Yes (1)
Myricitrin	2.753	3.551	No	No	0.285	2.972	No (2)
Quercetin	2.562	1.735	No	No	0.314	0.878	Yes (0)
Spinasterol	3.854	1.048	No	No	0.441	-1.156	Yes (1)

7UJQ

Figure 3: Aesculin's binding interaction and docking scores (PDB ID: 7UJO)

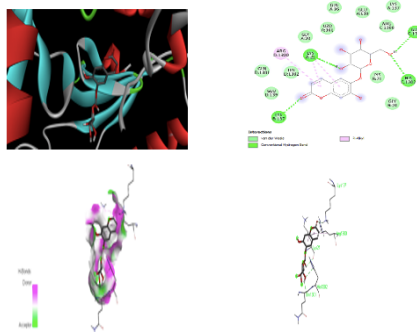


Figure 4. Catechin binding interaction and docking scores (PDB ID: 7UJQ)

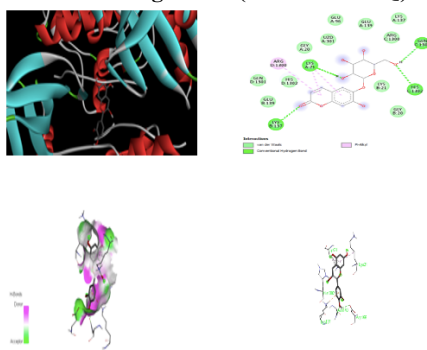


Figure 5: Myricetin binding interaction and docking scores (PDB ID: 7UJO)

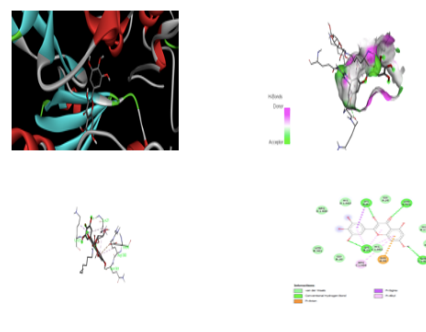


Figure 6. Myricitrin binding interaction and docking scores (PDB ID: 7UJQ)

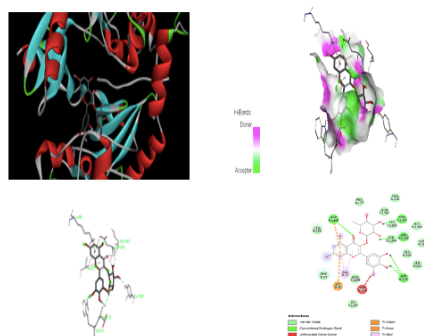


Figure 7. Quercetin binding interaction and docking scores (PDB ID: 7UJQ)

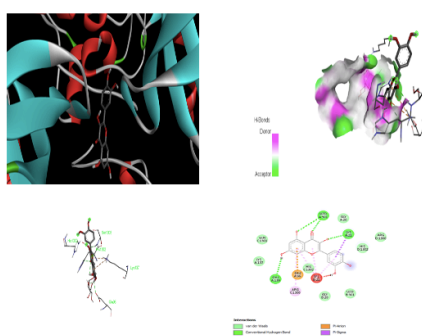
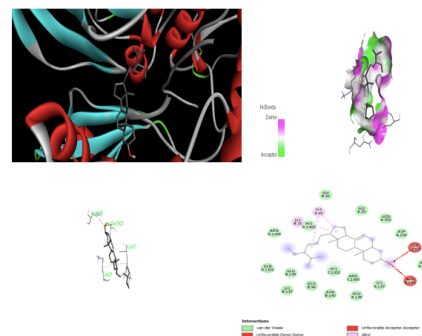


Figure 8. Spinasterol binding interaction and docking scores (PDB ID: 7UJQ)



708V

Figure 9: Aesculin binding interaction and docking scores (PDB ID: 7Q8V)

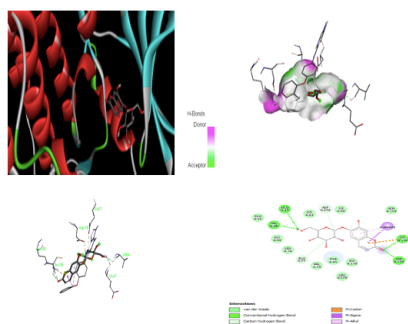


Figure 10. Catechin binding interaction and docking scores (PDB ID: 7Q8V)

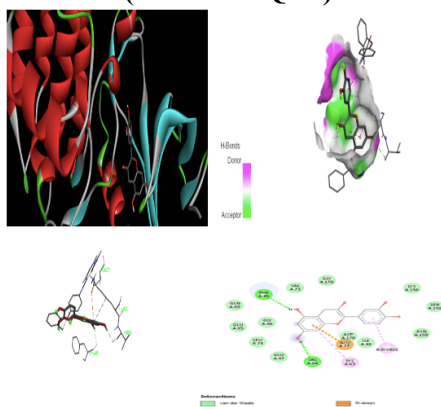


Figure 11. Myricetin binding interaction and docking scores (PDB ID: 7Q8V)

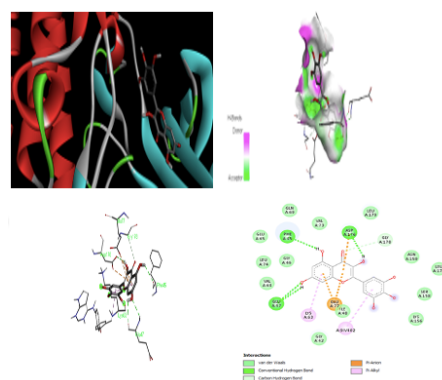


Figure 12. Myricetin binding interaction and docking scores (PDB ID: 7O8V)

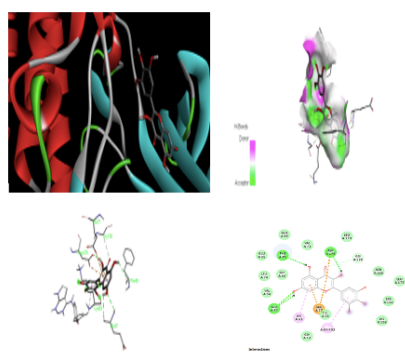


Figure 13. Quercetin binding interaction and docking scores (PDB ID: 7O8V)

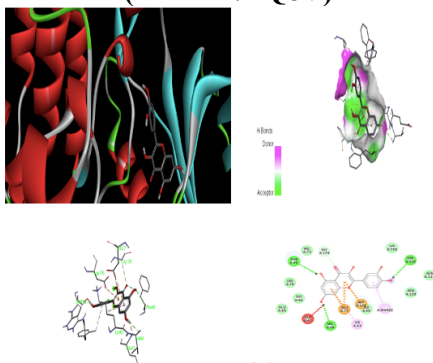


Figure 14. Spinasterol binding interaction and docking scores (PDB ID: 7Q8V)

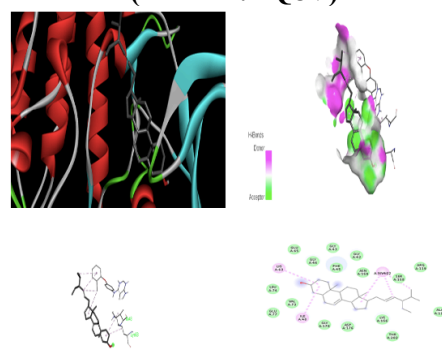


Diagram of a Boiled Egg

Figure 15: A representation of all the phytoconstituents combined with a standard boiled egg.

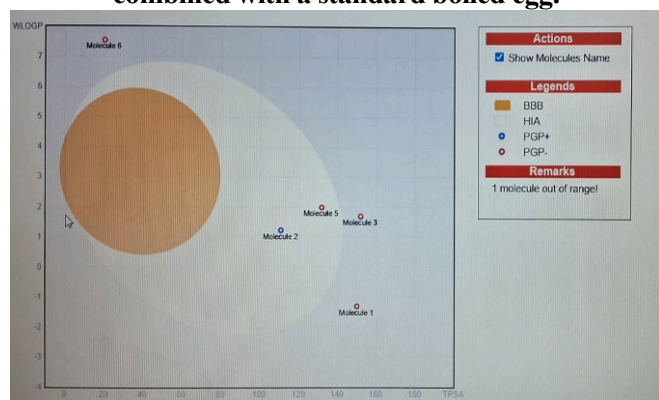


Table 4. Molecule names in boiled egg diagram

Molecule No	Phytochemicals
1	Aesculin
2	Catechin
3	Myricetin
4	Myricitrin
5	Quercetin
6	Spinasterol

The acronym for Brain or Intestinal Estimate D Permeation is Boiled the predictive model:

Two areas are depicted White and yellow in the diagram of a boiled egg. The physiochemical space of molecules likely to be absorbed via the whitish area is the gastrointestinal tract. while the physiochemical space of molecules most likely to enter the brain is the yellow region (yolk). Additionally, if the points are projected to be activated by P-gp (PGP+) efflux, they are colored blue. They become red if they are thought to be a non-substrate of P-gp (PGP).

Conclusion

In this study, we screened the phytoconstituents of the *Mimusops elengi* plant *in-silico*. Aesculin, catechin, myricetin, myricitrin, quercetin, and spinasterol are the six chemicals from the *Mimusops elengi* plant that were shown in this study. In 7UJQ and 7Q8V, the chosen phytocompounds had docking scores between -9.7 and -8.1 kcal/mol and between -9.9 and -7.7. In combination with 7UJQ & 7Q8V, spinasterol & myricitrin provided the highest binding energy (-9.7 & -9.9 kcal/mol) of all. These ligands also show favorable ADMET characteristics. In conclusion, the phytoconstituents found in *Mimusops elengi* have potent anti-7UJQ and 7Q8V properties. They may also be further studied for their immunosuppressive properties and for the creation of less harmful pharmaceuticals used to treat Alzheimer's disease.

References

- Castellani RJ, Rolston RK, Smith MA. Alzheimer disease. Disease-a-Month. 2010;56(9):484–546.

- Annaert WIM, Cupers P, Saftig P, De Strooper B. Presenilin function in APP processing. Ann N Y Acad Sci. 2000;920:158–64.
- Silvestrelli G, Lanari A, Parnetti L, Tomassoni D, Amenta F. Treatment of Alzheimer's disease: From pharmacology to a better understanding of disease pathophysiology. Mech Ageing Dev. 2006;127(2):148–57.
- Caroline dos Santos Picanço L, Farias Ozela P, de Fátima de Brito Brito M, Alves Pinheiro A, Carvalho Padilha E, Sarges Braga F, et al. Alzheimer's Disease: A Review from the Pathophysiology to Diagnosis, New Perspectives for Pharmacological Treatment. Curr Med Chem. 2017;24:1–19.
- Bonda DJ, Wang X, Perry G, Nunomura A, Tabaton M, Zhu X, et al. Oxidative stress in Alzheimer disease: A possibility for prevention. Neuropharmacology [Internet]. 2010;59(4–5):290–4. Available from: <http://dx.doi.org/10.1016/j.neuropharm.2010.04.005>
- Easton A, Sankaranarayanan S, Tanghe A, Terwel D, Lin AX, Hoque N, et al. Effects of sub-chronic donepezil on brain Abeta and cognition in a mouse model of Alzheimer's disease. Psychopharmacology (Berl). 2013;230(2):279–89.
- Lu C, Guo Y, Yan J, Luo Z, Luo H Bin, Yan M, et al. <https://doi.org/10.1021/Jm400567S>. J Med Chem. 2013;56(14):5843–59.
- Richardson C, Gard PR, Klugman A, Isaac M, Tabet N. Blood pro-inflammatory cytokines in Alzheimer's disease in relation to the use of acetylcholinesterase inhibitors. Int J Geriatr Psychiatry. 2013;28(12):1312–7.
- Lan XY, Liang DX, Yan S, Yang K. The design of control and data acquisition system for IXS experiment in SSRF. Hedianzixue Yu Tance Jishu/ Nuclear Electron Detect Technol. 2016;36(5):475–8.
- Dhapola R, Sarma P, Medhi B, Prakash A, Reddy DHK. Recent Advances in Molecular Pathways and Therapeutic Implications Targeting Mitochondrial Dysfunction for Alzheimer's Disease. Mol Neurobiol [Internet]. 2022;59(1):535–55. Available from: <https://doi.org/10.1007/s12035-021-02612-6>
- Yiannopoulou KG, Papageorgiou SG. Current and Future Treatments in Alzheimer Disease: An Update. J Cent Nerv Syst Dis. 2020;12.
- Gami B, Pathak S, Parabia M. Ethnobotanical , phytochemical and pharmacological review of *Mimusops*. Asian Pac J Trop Biomed [Internet]. 2012;2(9):743–8. Available from: [http://dx.doi.org/10.1016/S2221-1691\(12\)60221-4](http://dx.doi.org/10.1016/S2221-1691(12)60221-4)
- Roqaiya M, Begum W, Majeedi SF, Saiyed A. A review on traditional uses and phytochemical properties of *Mimusops elengi* Linn. 20 ~ Int J Herb Med. 2015;2(6):20–3.
- Kadam PV, Yadav KN, Deoda RS, Shivatare RS, Patil MJ. *Mimusops elengi* : A Review on Ethnobotany , Phytochemical and Pharmacological Profile. J Pharmacogn Phytochem. 2012;1(3):64–74.

15. Sayed DF, Afifi AH, Temraz A, Ahmed AH. Metabolic Profiling of *Mimusops elengi* Linn. Leaves extract and in silico anti-inflammatory assessment targeting NLRP3 inflammasome. Arab J Chem [Internet]. 2023;16(6):104753. Available from: <https://doi.org/10.1016/j.arabjc.2023.104753>
16. Shahwar D, Raza MA. Antioxidant potential of phenolic extracts of *Mimusops elengi*. Asian Pac J Trop Biomed [Internet]. 2012;2(7):547–50. Available from: [http://dx.doi.org/10.1016/S2221-1691\(12\)60094-X](http://dx.doi.org/10.1016/S2221-1691(12)60094-X)
17. Kar B, Kumar RBS, Karmakar I, Dola N, Bala A, Mazumder UK, et al. Antioxidant and in vitro anti-inflammatory activities of *Mimusops elengi* leaves. Asian Pac J Trop Biomed. 2012;2(2 SUPPL.).
18. Maulinda L, Husin H, Arahman N, Rosnelly CM, Syukri M, Nurhazanah, et al. The Influence of Pyrolysis Time and Temperature on the Composition and Properties of Bio-Oil Prepared from Tanjong Leaves (*Mimusops elengi*). Sustain. 2023;15(18):1–17.
19. GR S, S P, J R. Biodiesel Production from the Seeds of *Mimusops elengi* Using Potassium Aluminium Silicate as Novel Catalyst. Innov Energy Res. 2017;06(02):2–4.
20. Husin H, Abubakar A, Ramadhani S, Sijabat CFB, Hasfita F. Coconut husk ash as heterogenous catalyst for biodiesel production from cerbera manghas seed oil. MATEC Web Conf. 2018;197:2–5.
21. Srivastava R, Shukla G, Sharma S. Phytomedicinal importance of *Mimusops elengi*: an emerging present and promising future. Innoriginal Int J Sci. 2017;4(1).
22. Jahan J N, Ahmed W, Malik A. and H.E.J. Research Institute of Chemistry, University of Karachi, Karachi 75 270, Pakistan, “A Lupene-Type Triterpene From *Mimusops Elengi*,” journal-article, 1995.
23. Sen S, Sahu NP, Mahato SB. Novel migrated oleanane triterpenoid sapogenins from *mimusops elengi*. Tetrahedron. 1993;49(40):9031–8.
24. Sen S, Sahu NP, Mahato SB. Pentacyclic triterpenoids from *Mimusops elengi*. Phytochemistry. 1995;38(1):205–7.
25. Jahan N, Ahmed W, Malik A. A lupene-type triterpene from *Mimusops elengi*. Phytochemistry. 1995;39(1):255–7.
26. Allouche A rahman. Software News and Updates Gabedit — A Graphical User Interface for Computational Chemistry Softwares. J Comput Chem. 2012;32:174–82.
27. Verdonk ML, Cole JC, Hartshorn MJ, Murray CW, Taylor RD. Improved Protein – Ligand Docking Using GOLD. 2003;623(November 2002):609–23.
28. Leach AR, Shoichet BK, Peishoff CE. Docking and Scoring Perspecti V e. 2006;49(20).
29. Arora S, Lohiya G, Moharir K, Shah S, Yende S. Identification of Potential Flavonoid Inhibitors of the SARS-CoV-2 Main Protease 6YNQ : A Molecular Docking Study. Digit Chinese Med [Internet]. 2020;3(4):239–48. Available from: <http://dx.doi.org/10.1016/j.dcm.2020.12.003>
30. Shah S, Chaple D, Arora S, Yende S, Moharir K, Lohiya G. Exploring the active constituents of *Oroxylum indicum* in intervention of novel coronavirus (COVID - 19) based on molecular docking method. Netw Model Anal Heal Informatics Bioinforma [Internet]. 2021;10(1):1–12. Available from: <https://doi.org/10.1007/s13721-020-00279-y>
31. Kaloni D, Chakraborty D, Tiwari A, Biswas S. I P re of. Perspect Med [Internet]. 2020;100396. Available from: <https://doi.org/10.1016/j.hermed.2020.100396>
32. Joshi T, Sharma P, Joshi T, Chandra S. Ac ce pt. 2019;1102.
33. Nisha CM, Kumar A, Vimal A, Bai BM, Pal D, Kumar A. Docking and ADMET prediction of few GSK-3 inhibitors divulges 6-bromoindirubin-3-oxime as a potential inhibitor. J Mol Graph Model [Internet]. 2016; Available from: <http://dx.doi.org/10.1016/j.jm.2016.03.001>
34. Tsujimura S, Tanaka Y. Wj e m. 2015;5(4).
